





Article

CHA-Type Zeolite Prepared by Interzeolite Conversion Method Using FAU and LTL-Type Zeolite: Effect of the Raw Materials on the Crystallization Mechanism, and Physicochemical and Catalytic Properties

Toshiki Nishitoba ¹, Takuya Nozaki ¹, Sungsik Park ¹, Yong Wang ¹, Junko N. Kondo ¹, Hermann Gies ^{2,3} and Toshiyuki Yokoi ^{1,3,*}

¹ Institute of Innovative Research, Tokyo Institute of Technology, 4259 Nagatsuta, Midori-ku, Yokohama 226-8503, Japan; nishitoba.t@aist.go.jp (T.N.); nozaki.t.ad@m.titech.ac.jp (T.N.); park.s.ak@m.titech.ac.jp (S.P.); wangyong347@126.com (Y.W.); jnomura@res.titech.ac.jp (J.N.K.)

² Institute of Geology, Mineralogy und Geophysics, Ruhr-University Bochum, 44780 Bochum, Germany; hermann.gies@rub.de

³ Tokyo Tech World Research Hub Initiative (WRHI), Institute of Innovative Research, Tokyo Institute of Technology, 4259 Nagatsuta, Midori-ku, Yokohama 226-8503, Japan

* Correspondence: yokoi@cat.res.titech.ac.jp; Tel.: +81-45-924-5430; Fax: +81-45-924-5431

Received: 22 September 2020; Accepted: 14 October 2020; Published: 17 October 2020



Abstract: The effect of the raw materials including parent zeolite as aluminosilicate sources and organic structure-directing agents (OSDAs) on the crystallization mechanism, and physicochemical and catalytic properties of the CHA-type aluminosilicate zeolite was investigated. For this purpose, the FAU-type and the LTL-type zeolites were used as raw material, and trimethyladamantyl ammonium hydroxide and tetraethyl ammonium hydroxide were used as OSDAs. We firstly found that the CHA-type aluminosilicate zeolite was crystallized from the combination of the LTL-type zeolite and tetraethyl ammonium hydroxide as raw materials. The crystallization behaviors were also monitored in detail. The crystallization was delayed by using the LTL-type zeolite as the starting material regardless of the type of OSDA because of the low solubility of the LTL-type zeolite compared to the FAU-type zeolite. We have found that the Al distribution in the CHA framework was dependent on the raw materials. Thus, the prepared CHA-type aluminosilicate zeolite from the LTL-type zeolite exhibited a high thermal stability and catalytic performance in the methanol to olefins reaction.

Keywords: interzeolite conversion method; CHA-type zeolite; LTL-type zeolite; crystallization mechanism; MTO reaction

1. Introduction

An 8-membered ring (8-MR) zeolite such as CHA-type zeolites show an excellent activity for selective catalysis due to their small pores [1–27]. In 1985, the CHA-type aluminosilicate zeolite (hereinafter called CHA) was artificially synthesized by using FAU-type aluminosilicate zeolite (hereinafter called FAU) as raw material with potassium cation [6]. Thus, synthesized CHA has the Si/Al ratio of 2.0–4.0 in a framework. A high-silica type CHA (Si/Al = 5–150) has successfully been synthesized with the assistance of trimethyladamantyl ammonium cation (TMAda⁺) as an organic structure-directing agent (OSDA) [7]. Furthermore, fluoride and dry-gel conversion methods lead to the crystallization of the siliceous CHA-type framework without Al atoms [8,9]. Thus, the Si/Al ratio in CHA has been controlled in a wide range to date [10–15]. In addition to TMAda⁺, other

OSDAs including tetraethylammonium cation (TEA^+) [22,23] and benzyltrimethyl ammonium cation (BTMA^+) [18–21] have been applied in the synthesis of CHA.

Recently, besides FAU, various zeolites have been used as raw material via the so-called “interzeolite conversion (IZC)” method [16–30]. CHA has been synthesized with a short crystallization time using FAU- and PHI-type zeolites as raw material in the presence of TMAda^+ [16,17]. CHA has also been synthesized using LTL-type aluminosilicate zeolite (hereinafter called LTL) in the presence of TMAda^+ [28,29]. In addition to the type of zeolite as raw material, the influence of OSDA on the composition of the final product has been studied [31,32]. The combination of FAU and BTMA^+ has led to the synthesis of CHA with the Si/Al ratio ranging from 14 to 30 [18–21]. The use of TEA^+ has resulted in the synthesis of CHA with the Si/Al ratio ranging from 4.8 to 8.3 [22,23]. Nowadays, besides CHA-type zeolites, several zeolites have been synthesized from various zeolites as raw materials [33–38]. The *BEA-type zeolite has been converted into FAU [33], and the MFI-type zeolite has been synthesized using the *BEA-type zeolite as the starting material [34]. In the IZC method, structural units with local ordered structure, so-called “nano parts”, which are produced from zeolite as the starting material, play an important role in crystallizing the targeted zeolite [35–41].

More recently, in the synthesis of CHA via the IZC method using FAU (Si/Al = 2.8), we have found that the proportion of FAU in the raw materials strongly affected the distribution framework of Al atoms; when the proportion of FAU was high, the $\text{Q}^4(2\text{Al})$ -rich CHA, where “ $\text{Q}^4(n\text{Al})$ ” is $\text{Si}(\text{OSi})_{4-n}(\text{OAl})_n$, was obtained [42]. In addition to the proportion of FAU, the types of parent zeolite and/or OSDA will affect the physicochemical properties of the resultant CHA. Although the synthesis of zeolites using the IZC method has been reported by several groups, there are few reports on the relationship between the type of parent zeolite and the organic structure-regulating agent.

Here, we report on a new route to synthesize CHA-type aluminosilicate zeolite by the interzeolite conversion method using the LTL-type zeolite. Based on this new synthesis route, the effect of the raw materials including parent zeolite as an aluminosilicate sources and organic structure-directing agent (OSDA) on the crystallization mechanism, and physicochemical and catalytic properties was investigated. For these purposes, FAU and LTL were used as raw materials, and TMAdaOH and TEAOH were used as OSDA. The crystallization behaviors were also monitored in detail. Finally, the catalytic properties for the methanol to olefins (MTO) reaction were investigated.

2. Results

2.1. Synthesis of CHA-Type Zeolite

The CHA-type aluminosilicate zeolites were synthesized by using FAU and LTL via the IZC method in the presence of TMAda^+ as OSDA; the obtained products using FAU and LTL as starting material were designated as CHA–FAU– TMAda and CHA–LTL– TMAda , respectively. The Si/Al ratio in gel was set at 15. The XRD patterns of the calcined products revealed that all the products had a pure CHA phase (Figure S2 (Supplementary Materials)). The Si/Al ratios in the products are listed in Table 1. When TMAda^+ was used as the OSDA, the Si/Al ratios in CHA–FAU– TMAda and CHA–LTL– TMAda were 14.6 and 16.3, respectively, being almost in accordance with that in gel. In this case, the yields of the products, which were calculated by the weight of the as-synthesized product excluded from the organic content, were 94 and 84 wt %, respectively. On the other hand, the use of TEAOH resulted in the formation of CHA with a low yield and low Si/Al ratio compared to that of TMAdaOH . The Si/Al ratios synthesized with LTL and FAU were 10.5 and 6.3, respectively (designated as “CHA–LTL– TEA^+ ” and “CHA–FAU– TEA^+ ”, respectively). The yields of the products synthesized with TEAOH were much lower than those with TMAdaOH (ca. below 50%). In addition, in the case of CHA–LTL– TEA^+ , the crystallization of the CHA structure proceeds after the dissolution of LTL, as described later, and the crystallization is progressed by the IZC method.

Table 1. Physicochemical properties of the as-made samples.

Sample	in Gel				Yield/%	Si/Al	Na ⁺ /Al	K ⁺ /Al	(Na ⁺ + K ⁺)/Al	SDA/Al
	Si/Al	Na/Si	K/Si	SDA/Si						
CHA-LTL-TMAda	15	0.3	0.0	0.2	84	16.3	0.07	0.06	0.07	1.02
CHA-FAU-TMAda	15	0.3	0.0	0.2	94	14.6	0.12	-	0.12	1.10
CHA-LTL-TEA	15	0.3	0.1	0.55	49	10.5	0.05	0.16	0.21	0.78
CHA-FAU-TEA	15	0.3	0.1	0.55	40	6.3	0.36	0.18	0.54	0.23

The crystallization time was 120 h and the temperature was 443 K.

There were differences in the (Na⁺ + K⁺)/Al and OSDA/Al ratios among the products (Table 1). The OSDA/Al ratios in gels containing TMAdaOH and TEOH were 0.2 and 0.55, respectively. Nevertheless, the use of TEOH resulted in the formation of CHA with a low OSDA/Al compared to that of TMAdaOH. In the synthesis of CHA via the IZC method in the presence of OSDA, parent zeolite as a silica and alumina source is considered to be re-crystallized into the targeted structure being accompanying by OSDA as well as Na and K [31]. TMAda⁺ molecule was more effectively incorporated into the final product. This is because TMAda⁺, which has a higher C/N ratio than TEA⁺, would be easily combined with the amorphous aluminosilicate species produced from the parent zeolites through hydrophobic interaction [31]. Note that the OSDA/Al ratio for CHA-FAU-TEA (ca. 0.23) was much lower than that for CHA-LTL-TEA (ca. 0.78). This would be caused by the high loadings of Na and K in place of OSDA, and a higher dissolubility of FAU than LTL (described below). Thus, our results suggest that OSDA greatly affects the composition of the final products, and that the crystal growth process would be different depending on the combination of the parent zeolite and OSDA.

2.2. Evaluation of Al Species in CHA Structure

The ²⁷Al MAS NMR spectra of the calcined products are shown in Figure S3 (Supplementary Materials). A strong peak at 58 ppm assignment to the tetrahedral coordinated Al atoms in an oxygen environment. Furthermore, the peak at 0 ppm, which is assigned to octahedrally coordinated extra-framework Al atoms, was hardly observed. These results show mostly Al species in the products included in the CHA framework.

The ²⁹Si MAS NMR technique was applied to investigate the distribution of framework Al (Figure 1) [42]. All the spectra showed two peaks at −110 and −105 ppm, which correspond to Q⁴(0Al) and Q⁴(1Al), respectively, where Q⁴(nAl) is Si(OSi)_{4−n}(OAl)_n. Note that a broad peak around −100 ppm was observed, and it consists of two peaks at −101 and −99 ppm, which were assigned to Q⁴(2Al) and Q³(0Al), respectively, where Q³(nAl) is Si(OH)(OSi)_{3−n}(OAl)_n, respectively [43]. The proportions of the Si species estimated by deconvolution are listed in Table 2. When TMAdaOH was used as the OSDA, the proportion of Q³(0Al), the structural defect sites, was significantly high compared to the use of TEOH. In these cases, the excess amounts of Na and OSDA species in comparison with the Al content were loaded; the (Na + OSDA)/Al ratios for CHA-LTL-TMAda and CHA-FAU-TMAda were calculated to be 1.09 and 1.22, respectively (Table 1). Thus, excess loadings would cause the formation of the negatively charged defect sites, resulting in the high proportion of Q³(0Al).

Interestingly, there was a marked difference in the Al distribution among the products; the Q⁴(2Al)/Q⁴(1Al) ratio was dependent on the type of zeolite used, not OSDA. Note that CHA-LTL-TEA was the lowest (ca. 0.05). The use of FAU resulted in a high Q⁴(2Al)/Q⁴(1Al) ratio compared to that of LTL. The FAU used as the parent zeolite had a high proportion of Q⁴(2Al) compared to LTL (Figure S1 (Supplementary Materials)). Thus, the amorphous aluminosilicate species produced from FAU would contain a high proportion of Q⁴(2Al), resulting in the Q⁴(2Al)/Q⁴(1Al) ratio in the products. These results indicate that the raw materials including parent zeolite strongly affected the Al distribution.

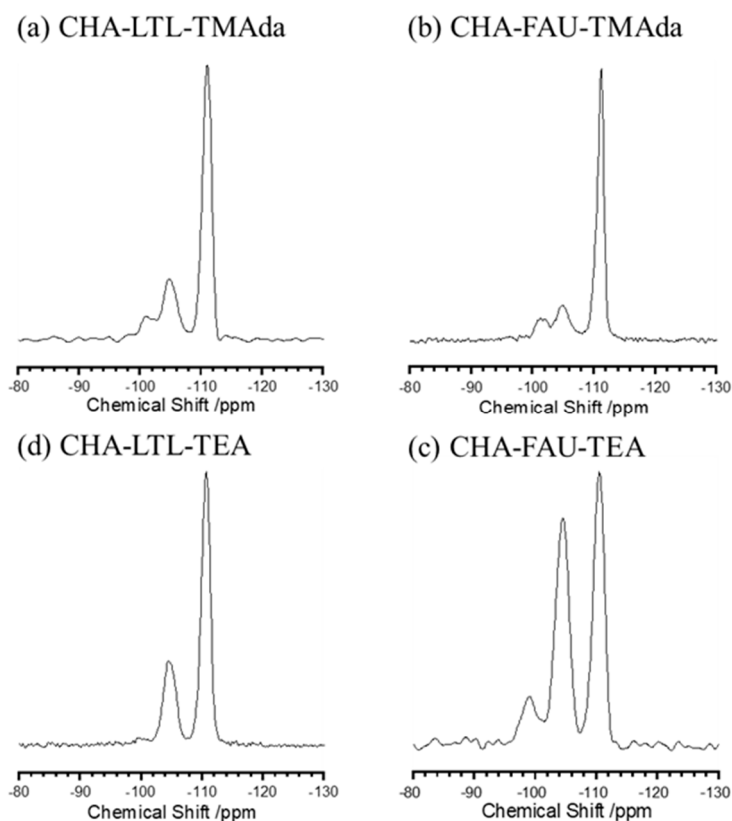


Figure 1. ^{29}Si MAS NMR spectra with curve fittings of the products: (a) CHA-LTL-TMAda, (b) CHA-FAU-TMAda, (c) CHA-LTL-TEA, (d) CHA-FAU-TEA. TEA: Tetraethylammonium cation; TMAda: Trymethyladamantyl ammonium cation.

Table 2. ^{29}Si MAS NMR spectra deconvolution results.

Sample	Si/Al (ICP)	Si/Al ^a (NMR)	Proportion of Q ⁴ (nAl) ^b and Q ³ (nAl) ^c /%					Q ⁴ (2Al)/Q ⁴ (1Al)
			Q ⁴ (3Al)	Q ⁴ (2Al)	Q ⁴ (1Al)	Q ⁴ (0Al)	Q ³ (0Al)	
CHA-LTL-TMAda	16.3	14.7	<0.1	2.1	22.9	67.0	7.9	0.091
CHA-FAU-TMAda	14.6	19.6	<0.1	1.5	16.4	73.1	9	0.122
CHA-LTL-TEA	10.5	12.9	<0.1	1.3	28.4	69.1	1.2	0.046
CHA-FAU-TEA	6.3	6.2	<0.1	9.8	44.4	44.6	0.11	0.22

^a Si/Al_(NMR): Si/Al atomic ratio in the sample determined by ^{29}Si MAS NMR spectra. ^b Q⁴(nAl): Si(OSi)_{4-n}(OAl)_n.

^c Q³(nAl): Si(OSi)_{3-n}(OH)(OAl)_n.

2.3. Crystallization Behavior of CHA via the IZC Method Using FAU and LTL

2.3.1. Crystallinity

The crystallization behaviors were monitored in detail. The changes in the XRD patterns of the products along with crystallization time are shown in Figure 2. For CHA-LTL-TMAda and CHA-FAU-TMAda, the diffraction peaks of the parent zeolites (LTL and FAU) were clearly observed until 24 and 6 h, respectively. The crystallinity was estimated based on relative intensity, and the change in the crystallinity of the FAU, LTL and CHA phases along with the crystallization time are shown in Figure 3. In the synthesis from LTL, the crystallinity of LTL was gradually decreased along with the crystallization time, and the LTL phase mostly disappeared after 120 h irrespective of type of OSDA. The CHA phase was clearly observed after 24 h, and its crystallinity was dramatically increased at the crystallization time of 48 h. Finally, a pure CHA phase was obtained after 120 h. On the other hand, in the synthesis from FAU, the FAU phase was quickly decreased to below 20% at only 1 h irrespective of the type of OSDA, and almost 100% crystallinity of CHA was achieved within 24 h, and

the CHA phase was completely retained for 120 h. The pH values in the synthesis gels containing TMAdaOH and TEOAH were almost similar (ca. 13.2 and 13.6, respectively). Therefore, observed differences could be explained by the difference in the dissolubility between FAU and LTL, which is caused by the framework density: 13.3 and 16.7 T/1000 Å³ is for FAU and LTL, respectively. We have considered that FAU was quickly dissolved and produced more amorphous aluminosilicate species compared to LTL, and the produced amorphous aluminosilicate species were crystallized into the CHA phase in the presence of OSDA.

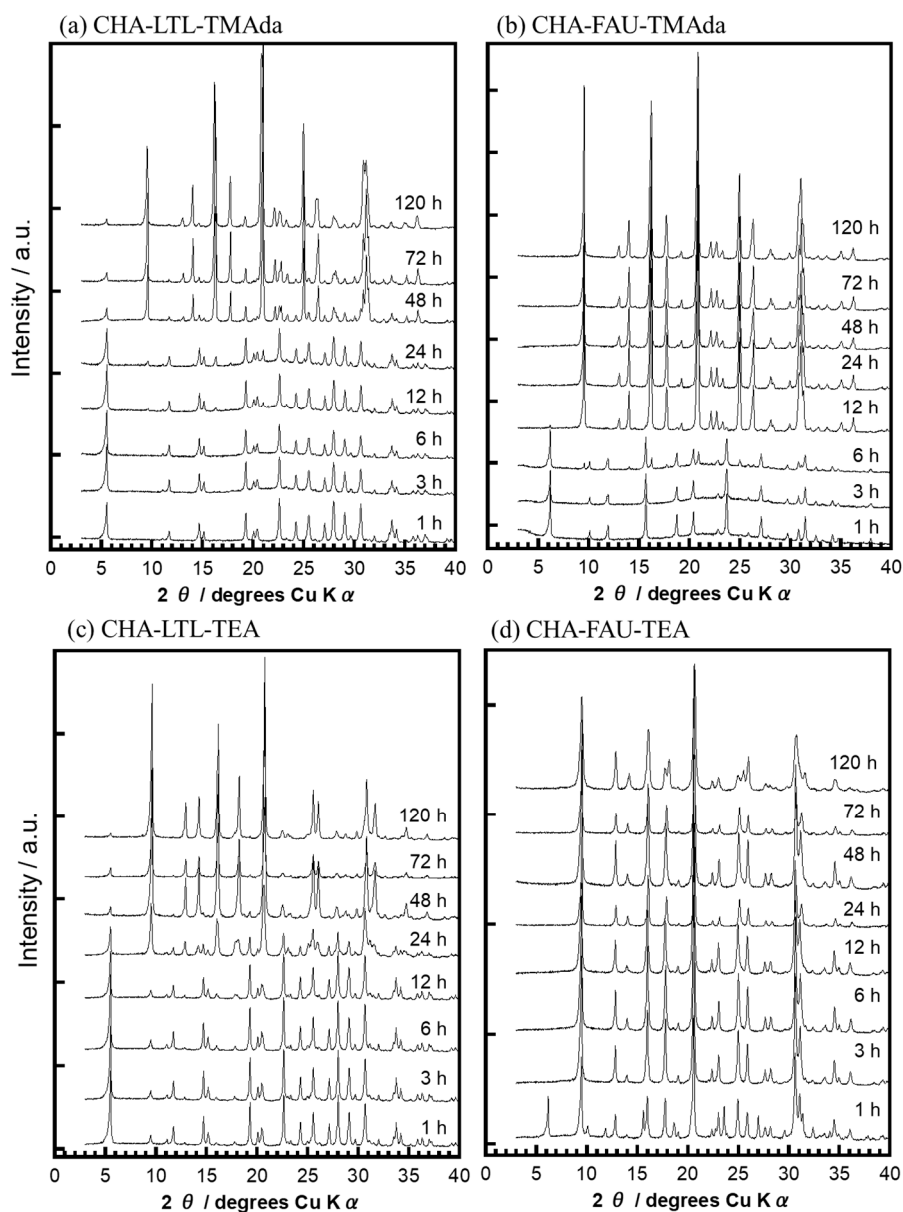


Figure 2. XRD patterns of (a) CHA-LTL-TMAda; (b) CHA-FAU-TMAda; (c) CHA-LTL-TEA and (d) CHA-FAU-TEA at different crystallization times.

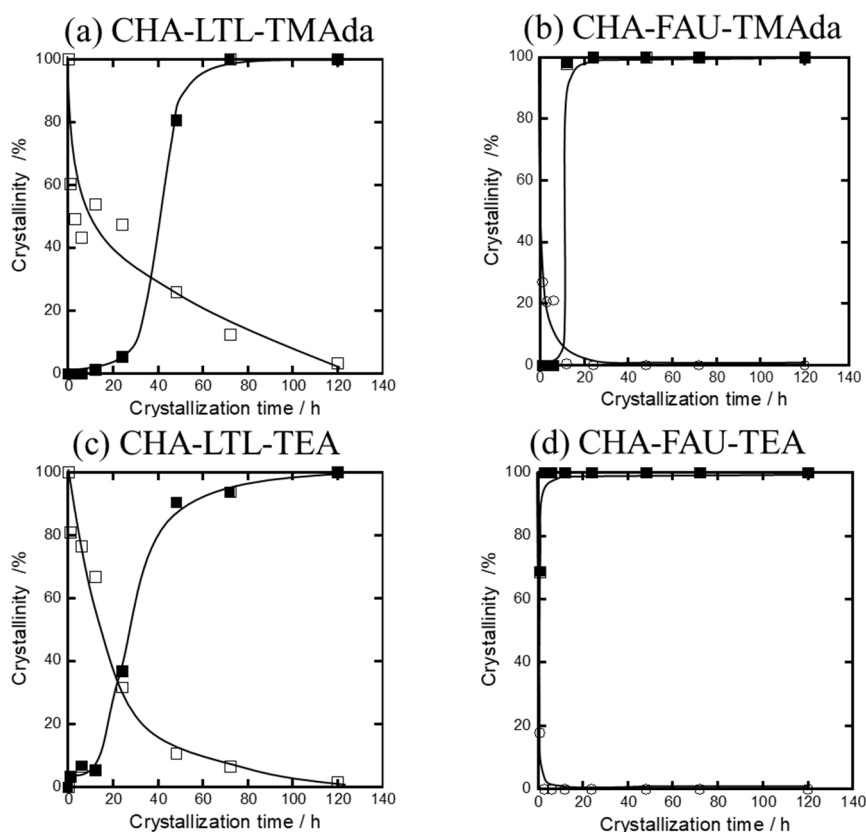


Figure 3. Relationship between crystallization time and crystallinity of LTL (□), FAU (○) and CHA (■). (a) CHA-LTL-TMAda, (b) CHA-FAU-TMAda, (c) CHA-LTL-TEA, (d) CHA-FAU-TEA.

2.3.2. Solid Yield and Al Content

The changes in the solid yield and Si/Al ratio along with crystallization time were investigated (Figure 4). When TMAdaOH was used as the OSDA, the Si/Al ratios of the solid products were dramatically increased when the formation of CHA started, and the Si/Al ratios in the final products were almost similar to that of the synthesis gel, irrespective of the parent zeolites. The yields were also increased along with the formation of CHA, and they reached over 94 and 84% for CHA-LTL-TMAda and CHA-FAU-TMAda, respectively. For CHA-LTL-TMAda, the yield and Si/Al ratio were gradually increased along with the crystallization time ranging from 12 to 72 h. The amorphous silicate species derived from LTL were consumed for the crystal growth. On the other hand, for CHA-FAU-TMAda, the yield and Si/Al ratio were unchanged after 24 h, suggesting that CHA was completely crystallized for 24 h.

When TEAOH was used as the OSDA, there was a clear difference in the change in the Si/Al ratio along with the crystallization time between CHA-LTL-TEA and CHA-FAU-TEA. When the crystallization time was increased from 24 to 72 h, the Si/Al ratio of CHA-LTL-TEA was increased from 3.2 to 10.5, and then it was unchanged after 72 h. For CHA-FAU-TEA, the yield was drastically increased to 31% for 12 h, and it finally reached 40%. Correspondingly, the Si/Al ratio was increased to 4.5 for 12 h, and it had a slight increase. It finally reached 6.3 at 120 h. These results imply that the crystallization of CHA was mostly completed within 12 h.

The changes in the amount of OSDA, Na^+ , and K^+ were also monitored in terms of the charge balance of zeolite framework. Figure 5 shows the changes in the amount of OSDA amount along with the crystallization time. For CHA-LTL-TMAda, the TMAdaOH in product was stable (ca. 0.4 mmol g^{-1}) until 24 h, and it was dramatically increased up to 0.8 at 48 h. It reached about 1.2 mmol g^{-1} at 72 h. For CHA-FAU-TMAda, the TMAdaOH/Al quickly reached 1.2 within 12 h, and it was almost unchanged after 12 h.

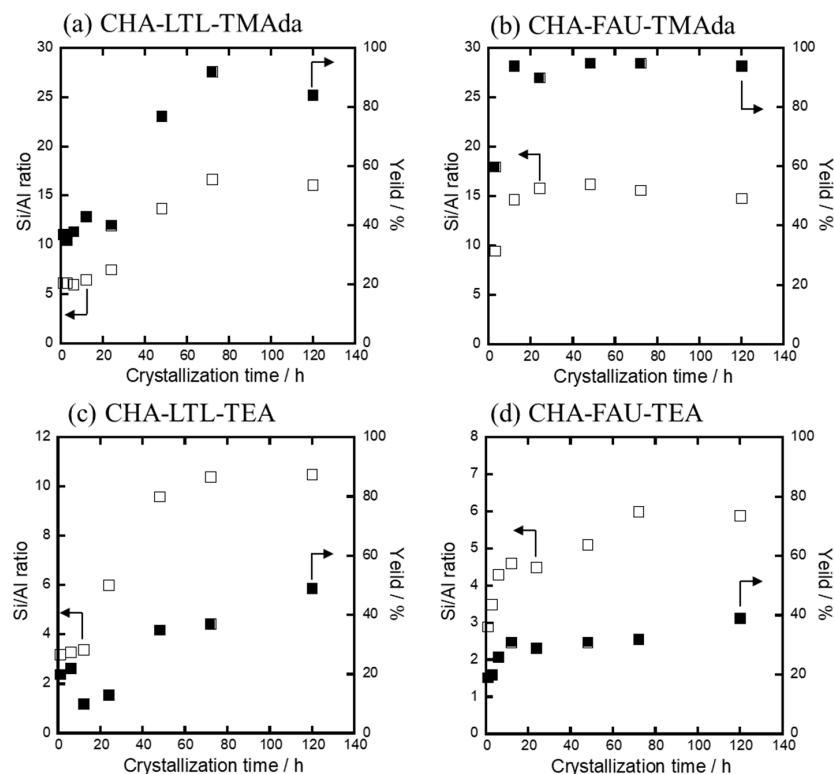


Figure 4. Relationship between crystallization time and yield (■) and Si/Al ratio (□). (a) CHA-LTL-TMAd, (b) CHA-FAU-TMAd, (c) CHA-LTL-TEA, (d) CHA-FAU-TEA.

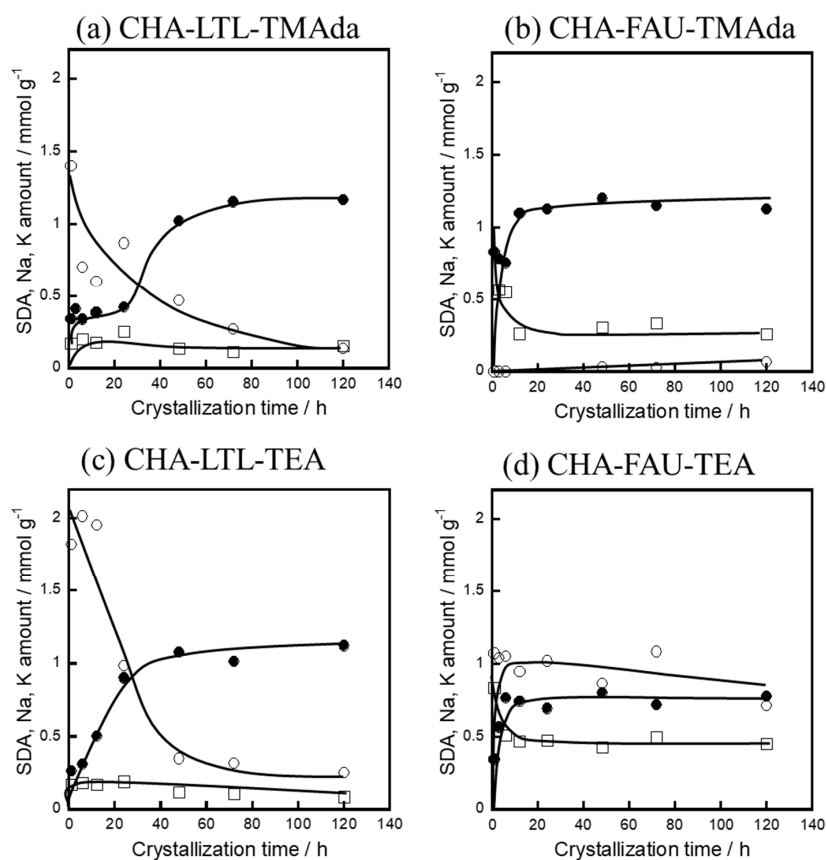


Figure 5. Relationship between crystallization time and SDA/Al. (a) CHA-LTL-TMAd, (b) CHA-FAU-TMAd, (c) CHA-LTL-TEA, (d) CHA-FAU-TEA (□: Na⁺, ○: K⁺, ●: OSDA).

The TEAOH/Al ratio in CHA–LTL–TEA was gradually increased to 0.78 for 72 h. On the other hand, that in CHA–FAU–TEA reached 0.2 within 6 h, and it was almost unchanged after 6 h. Thus, the behavior of the OSDA/Al ratio against the crystallization time was dependent on the type of the parent zeolites, not OSDA.

2.3.3. Particle Morphology

The changes in the particle morphology of the products along with the crystallization times ranging from 1 to 120 h were investigated (Figure 6). The SEM images of LTL and FAU used as starting material are shown Figure S1 (Supplementary Materials), showing cylindrical particles 0.2–0.3 μm and octahedral particles 0.8–1.0 μm in size, respectively. When TMAdaOH was used as OSDA, cubic particles about 5.0 μm in size were finally formed irrespective of the parent zeolites. At the initial stages of the crystallization until 3 h, particles attributed to the amorphous product were observed. The presence of an amorphous product was consistent with the observation of the so-called “halo peak” at 20° in the XRD measurement (Figure 1). The formation of the cubic particles began at 6 h (Figure 3a), and cubic particles were clearly observed at 12 h for CHA–FAU–TMAda, while amorphous particles were still observed for CHA–LTL–TMAda at this time

The particle size of CHA–FAU–TMAda was almost unchanged after 12 h. For CHA–LTL–TMAda, the formation of cubic particles began at 48 h, and it was almost completed at 72 h. There was not a marked difference in the particle size of the final products between CHA–LTL–TMAda and CHA–FAU–TMAda. So-called “hydrophobic effect” of TMAda⁺ species might enhance the interaction with amorphous aluminosilicate species derived from the parent zeolites. Such species would be involved in crystal growth, resulting in the formation of large crystals.

When TEAOH was used as OSDA, cubic particles 0.3–0.4 μm in size were observed at 3 h, and their formation was almost completed at 6 h for CHA–FAU–TEA. On the other hand, LTL were still observed until 6 h, the formation of cubic particles began at 24 h, and the particles gradually grew along with the crystallization time. Finally, stacked cubic particles 1.0 μm in size were formed at 120 h. Thus, in the use of TEAOH, the use of LTL led to the increase in the particle size.

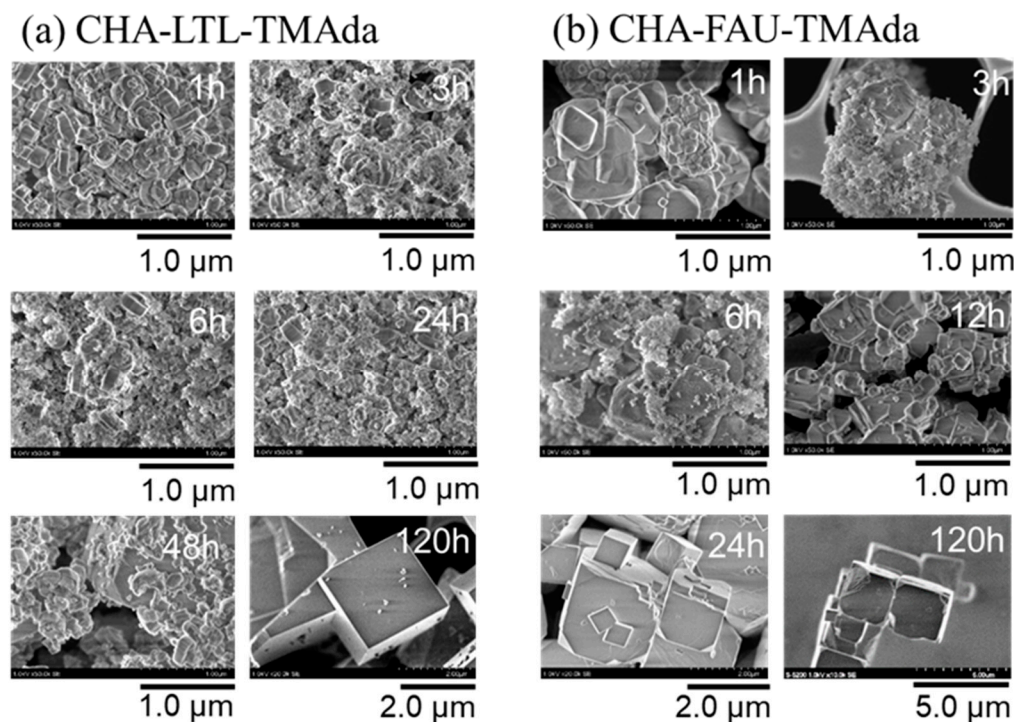


Figure 6. Cont.

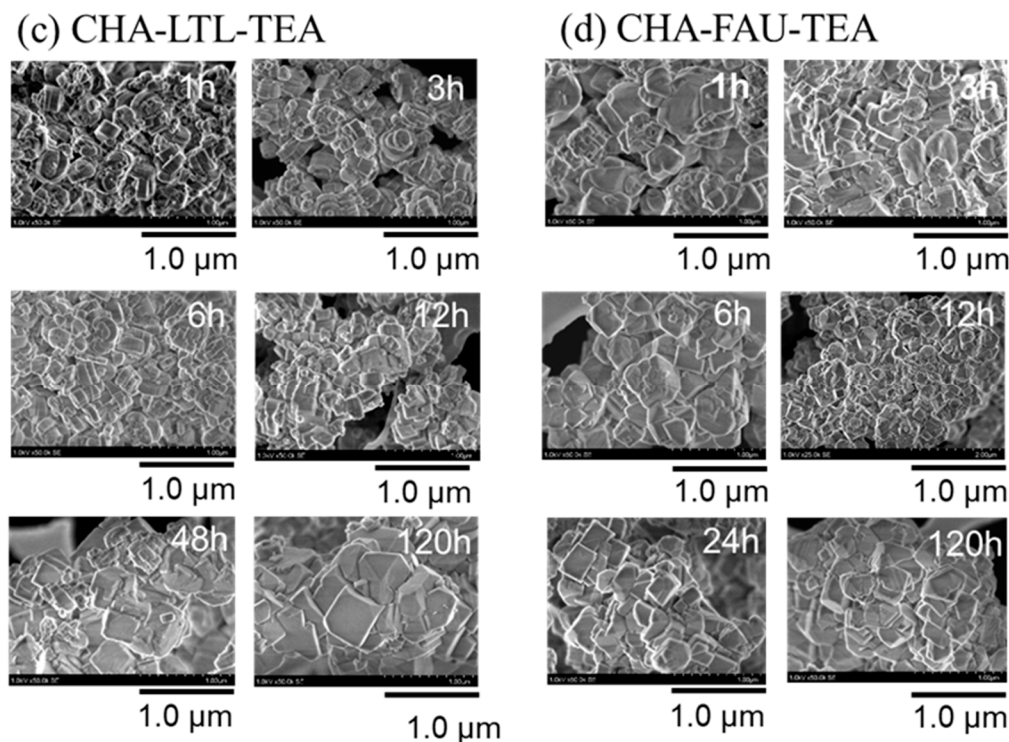


Figure 6. SEM images of (a) CHA-LTL-TMAda, (b) CHA-FAU-TMAda, (c) CHA-LTL-TEA, (d) CHA-FAU-TEA at different crystallization times.

These results indicated that the parent zeolite affected the nucleation of CHA. In the synthesis from FAU, FAU was quickly dissolved, forming “nanoparts” containing Na^+ and K^+ cations, which would enhance the nucleation of CHA [44–46]. On the other hand, the dissolution of LTL was slow, and the production of the nanoparts was also retarded. As a result, the nucleation of CHA would also be delayed, forming larger-sized CHA compared to the use of FAU.

2.4. Hydrothermal Stability

Hydrothermal stability is one of the most important properties of zeolite. The CHA samples synthesized from LTL are expected to show a high hydrothermal stability because they showed a high $\text{Q}^4(1\text{Al})$ proportion compared to those from FAU [42]. The XRD patterns of the NH_4^+ from samples before and after the hydrothermal treatment are shown in Figure 7. CHA-FAU-TEA was collapsed upon the hydrothermal treatment. It is well known that zeolite with a high Al content shows a poor hydrothermal stability because water vapor reacts easily with framework Al species, enhancing the cleavage of the Si–O–Al bond [47]. For CHA-LTL-TMAda and CHA-FAU-TMAda, the CHA structure was retained after the hydrothermal treatment, while the intensities were slightly decreased; the relative crystallinity was decreased to 73 and 49%, respectively. CHA-LTL-TMAda showed a slightly higher hydrothermal stability than CHA-LTL-TMAda in spite of a similar Si/Al ratio and particle size. Note that the relative crystallinity of CHA-LTL-TEA was almost unchanged after the hydrothermal treatment; the relative crystallinity was calculated to be 91%. The difference in the hydrothermal stability would be related to the Al distribution as well as the Al content. We have reported that the CHA-type zeolite with more $\text{Q}^4(1\text{Al})$ species and/or lower defect sites is more stable in hydrothermal conditions [42]. Considering that the use of FAU resulted in a high $\text{Q}^4(2\text{Al})/\text{Q}^4(1\text{Al})$ ratio compared to that of LTL (Table 2), it is successfully concluded that the high hydrothermal stability of CHA-LTL-TMAda and CHA-LTL-TEA is derived from a low $\text{Q}^4(2\text{Al})/\text{Q}^4(1\text{Al})$ ratio. Such properties would be advantageous for the application to the selective reduction of NO_x .

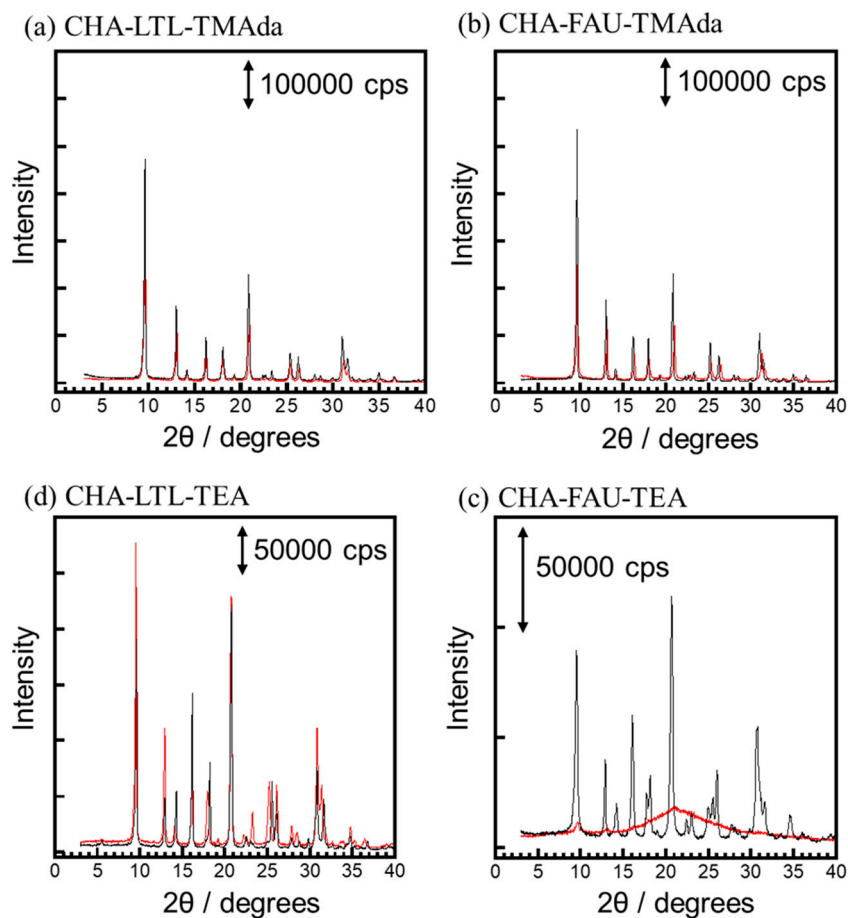


Figure 7. XRD patterns of before (black line) and after (red line) hydrothermal treatment of the samples. (a) CHA-LTL-TMAda, (b) CHA-FAU-TMAda, (c) CHA-LTL-TEA, (d) CHA-FAU-TEA.

2.5. MTO Reaction

The prepared CHA samples were used as catalyst for the MTO reaction. Figure 8 shows the change in the conversion of methanol and the products' selectivities along with time on stream (TOS) at 350 °C. Table S1 (Supplementary Materials) summarizes the products' selectivities when the selectivity to ethene was the highest in each sample. At the initial region (TOS = 10 min), for all the samples, the methanol conversion reached 100% and the main product was ethene followed by propene. The selectivity to ethene was increased along with the TOS until the deactivation started. Furthermore, dimethylether (DME) was formed after the deactivation started. Thus, the prepared CHA samples in this study exhibited similar catalytic properties to those in the literature [48,49]. The CHA catalysts synthesized using TMAdaOH, CHA-LTL-TMAda and CHA-FAU-TMAda showed a longer catalytic life and higher selectivity to light olefins compared to those synthesized using TEA, although the use of TMAdaOH resulted in the formation of larger particles (Table S1 (Supplementary Materials)). CHA-FAU-TEA showed the shortest catalytic life. The difference in the acid amount is one of the critical reasons for catalytic life (Table S1 (Supplementary Materials)). In addition, the distribution of framework Al would influence the catalytic properties described below.

In the MTO reaction, light olefins are produced by the cracking of alkanes and alkenes and the so-called "hydrocarbon pool mechanism" [50,51]. The higher yields of paraffins could be caused by the Lewis acid site derived from extra-framework Al species in the hydrogen transfer reactions [52,53]. Therefore, we investigated the Al state of the H⁺-type products (Figure S4 (Supplementary Materials)) in addition to the calcined Na⁺-type products (Figure S3 (Supplementary Materials)): Figures S3 and S4 (Supplementary Materials) revealed that the ion-exchange process resulted in the formation of

extra-framework Al species, in particular CHA-FAU-TEA. In addition, CHA-FAU-TEA gave the highest value for the $Q^4(2Al)/Q^4(1Al)$ ratio (Table 2). It has been reported that $Q^4(2Al)$ species would enhance hydrogen transfer reactions [12,42], accelerating aromatization followed by coke formation. Thus, CHA-FAU-TEA showed the shortest catalytic life (Figure 8).

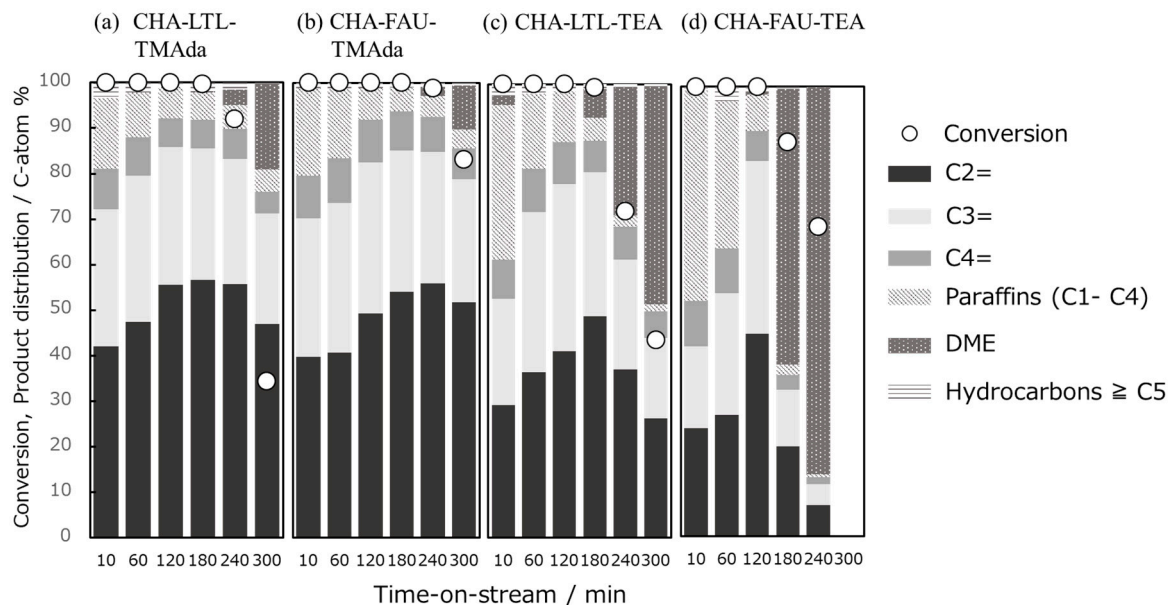


Figure 8. The methanol to olefins (MTO) reaction over (a) CHA-LTL-TMAda, (b) CHA-FAU-TMAda, (c) CHA-LTL-TEA, and (d) CHA-FAU-TEA.

3. Materials and Methods

3.1. Synthesis of CHA-Type Zeolite from FAU- and LTL-Type Zeolites

JRC-Y-4.8 (Si/Al = 2.4, Catalysis Society of Japan, Tokyo, Japan) and HSZ-500KOA (Si/Al = 3.0, Tosoh Corp., Tokyo, Japan) were used as FAU and LTL, respectively (Figure S1 (Supplementary Materials)). Two kinds of OSDA, tryethyladamantylammonium hydroxide (TMAdaOH) (SACHEM, Texas, USA) and tetraethylammonium hydroxide (TEAOH) (TCI 35% in water, Tokyo, Japan) were used. Fumed silica (Cab-O-Sil M5, CABOT, MA, USA) was added as an additional silica source to achieve the targeted composition of the mother gel.

In the presence of TMAdaOH, the molar ratio of the mother gel was 1 SiO₂/0.033 Al₂O₃/0.2 NaOH/0.2 TMAdaOH/40 H₂O. In this work, 15 mmol SiO₂ was applied to synthesize the CHA-type zeolite. The 10 wt % seed crystal (CHA-type zeolite synthesized by Ref. [24]) was added to the mother gel. After stirring at room temperature for 1 h, the mother gel was hydrothermally treated at 443 K in a stirring for 1–120 h for the evaluation of crystallization behavior. The solid product was recovered by filtration, washed with distilled water, and dried at 373 K. The sample was calcined under 873 K for 5 h in air. Then, the calcined Na-form sample was carried out the ion exchange at 353 K for 3 h using 2.0 M NH₄NO₃ aqueous solution. This treatment was repeated 3 times to convert into the NH₄-type. Finally, the H⁺-type was obtained after calcination of the NH₄-type under an air atmosphere at 873 K for 5 h. Thus, obtained products using FAU and LTL as starting materials were designated as CHA-FAU-TMAda and CHA-LTL-TMAda, respectively.

In the presence of TEAOH, the following system was used: 1 SiO₂/0.033 Al₂O₃/0.3 NaOH/0.1KOH/0.55 TEAOH/40 H₂O, and 15 mmol SiO₂ was also applied. The 10 wt % seed crystal was added to the mother gel. The prepared mother gel was hydrothermally treated, and then the H-type form was obtained by the method similar to the use of TMAdaOH. The products were designated as CHA-FAU-TEA and CHA-LTL-TEA.

3.2. Characterization

X-ray diffraction (XRD) patterns were collected on a Rint-Ultima III (Rigaku, Tokyo, Japan) using a CuK α X-ray source (40 kV, 20 mA). The crystallinity was calculated based on the relative intensity, which was estimated as follows.

$$\text{Relative crystallinity of LTL, FAU} = \frac{\text{The sum of the peak intensity of LTL, FAU at each crystallization time}}{\text{The sum of peak intensity of raw materials}} \quad (1)$$

$$\text{Relative crystallinity of CHA} = \frac{\text{The sum of peak intensity of CHA at each crystallization time}}{\text{The sum of peak intensity of CHA at 5days}} \quad (2)$$

Sum of peak intensity at 2 θ

LTL = 5.5°, 11.7°, 14.6°, 19.2°, 22.6°, 24.2°, 25.5°, 28.0°, 29.0° and 30.5°

FAU = 6.0°, 10.1°, 11.8°, 15.6°, 18.7°, 20.4°, 23.7°, 27.1° and 31.4°

CHA = 9.8°, 16.1°, 18.2°, 21.0°, 25.3°, 26.4° and 31.1°

FE-SEM images of the powder samples were collected on an S-5200 microscope (Hitachi, Tokyo, Japan). The amount of the Si and Al was analyzed by ICP-AES using a ICPE-9000 spectrometer (Shimadzu, Kyoto, Japan). The amount of Na and K in the samples was estimated by atomic absorption spectroscopy (AAS) on a AA-6200 spectrometer (Shimadzu, Kyoto, Japan). The amount of organic species in the as-synthesized samples was determined based on the weight loss from 573 to 1073 K in a thermogravimetric (TG) profile, which was performed on a thermogravimetric–differential thermal analyzer (TG-DTA, Thermo plus EVO II) (Rigaku, Tokyo, Japan). To determine the acid amount, temperature-programmed NH₃ desorption profiles (NH₃-TPD) were recorded on BEL-CAT (MicrotracBEL, Osaka, Japan). Solid-state NMR spectra were obtained on a JEOL ECA-600 spectrometer (14.1 T) (JEOL, Tokyo, Japan). The samples were spun at 15 kHz by using a 4 mm ZrO₂ rotor. For ²⁷Al MAS (Magic Angle Spinning) NMR spectra, the ²⁷Al chemical shift was referenced to −0.54 ppm, AlNH₄(SO₄)₂·12H₂O. For ²⁹Si MAS and ²⁹Si CP/MAS NMR spectra, the ²⁹Si chemical shift was referenced to −34.12 ppm using polydimethylsiloxane (PDMS)(Sigma-Aldrich, St. Louis, MO, USA).

3.3. Hydrothermal Stability

About 300 mg of binder-free zeolite pellets (50/80 mesh) were filled into a quartz-tube flow micro-reactor (inner diameter 6 mm) and heated from room temperature to 1073 K under air flow at a heating rate of 5 K min^{−1} with 40 vol % H₂O (P_{H2O} = 40.5 kPa, W/F = 1.62, N₂ balance), and the hydrothermal stability of the zeolite was investigated by hydrothermal treatment at 1073 K for 5 h. The stability was assessed based on the relative crystallinity, which is defined as the change in the sum of the intensities of the diffraction peaks assigned to the CHA structure.

3.4. MTO Reaction

The reaction was performed by using a continuous flow reactor at atmospheric pressure. The H⁺-form samples were pressed, crushed, and sorted into grains using 50/80 meshes without a binder. The grains were packed into a quartz tubular flow microreactor (6 mm inner diameter) in a vertical furnace and heated under helium from room temperature to 773 K. This temperature was maintained for 1 h prior to the reaction, and then cooled to the desired reaction temperature. The pressure of methanol was set at 5 kPa with He as a carrier gas. W/F for methanol was set at 34 g h mol^{−1}. Ethene, propene, butenes, C1–C4 paraffins, over-C5 hydrocarbons, and dimethyl ether (DME) were detected as products, which were analyzed by an online gas chromatograph GC-2014 (Shimadzu,

Kyoto, Japan) equipped with HP-PLOT/Q capillary column and an FID (flame ionization detector). The conversion of methanol and selectivity of the products was calculated by the formula below.

$$\text{Conversion of reactants} = 100 - \frac{\text{C - atoms of Methanol (output)}}{\text{C - atoms of Methanol (input)}} \times 100 \quad (3)$$

$$\text{product distribution} = \frac{\text{C - atoms of the product}}{(\text{C - atoms of Methanol (input)} - \text{C - atoms of Methanol (output)})} \times 100 \quad (4)$$

4. Conclusions

A new synthesis route of CHA-type aluminosilicate zeolite by the interzeolite conversion method using the LTL-type zeolite in the presence of tetraethyl ammonium hydroxide has successfully been developed. Based on this new synthesis route, the effect of the raw materials including parent zeolite as aluminosilicate sources and an organic structure-directing agent (OSDA) on the crystallization mechanism, and the physicochemical and catalytic properties, were investigated. We have found that OSDA greatly affects the composition of the final products, and that the raw materials strongly influenced the Al distribution in the final products; the use of FAU resulted in a high $Q^4(2Al)/Q^4(1Al)$ ratio compared to that of LTL. By monitoring the crystallization behaviors, the crystallization was delayed by using the LTL-type zeolite as raw material regardless of the type of organic structure-directing agent because of the low dissolubility of the LTL-type zeolite compared to the FAU-type zeolite.

The hydrothermal stability and catalytic performance in the MTO reaction of the prepared CHA-type zeolites were clearly dependent on the raw materials. The use of LTL-type zeolite as a raw material improved the hydrothermal stability, which is closely related to the Al distribution in the CHA framework. The CHA zeolites synthesized using TMAdaOH showed a longer catalytic life and higher selectivity to light olefins in the MTO reaction compared to those synthesized using TEA. The results obtained from this study clearly showed that the raw materials for the CHA-type zeolite should be optimized depending on its application. Furthermore, our findings will contribute to the diversification of the IZC method, to the improvement of hydrothermal stability of zeolite, and also to the control of the distribution of the heteroatoms in the zeolite framework.

Supplementary Materials: The following are available online at <http://www.mdpi.com/2073-4344/10/10/1204/s1>, Figure S1: Physicochemical properties of used as parent zeolite for the synthesis of CHA, Figure S2: XRD patterns of products, Figure S3: ^{27}Al MAS NMR spectra of the calcined Na^+ -type products, Figure S4: ^{27}Al MAS NMR spectra of the H^+ -type products, Table S1: The products' selectivities in the MTO reaction over products.

Author Contributions: Conceptualization, T.N. (Toshiki Nishitoba) and T.Y.; formal analysis, T.N. (Toshiki Nishitoba) and T.N. (Takuya Nozaki); funding acquisition, H.G. and T.Y.; investigation, T.N. (Toshiki Nishitoba), T.N. (Takuya Nozaki), S.P. and Y.W.; methodology, T.N. (Toshiki Nishitoba) and T.Y.; project administration, T.Y.; resources, J.N.K. and T.Y.; supervision, T.Y.; writing—original draft, T.N. (Toshiki Nishitoba) and T.Y.; writing—review and editing, S.P., Y.W., J.N.K., H.G. and Y.T. All authors have read and agreed to the published version of the manuscript.

Funding: This research received no external funding.

Acknowledgments: This work was supported by Tokyo Tech World Research Hub Initiative (WRHI) Program of Institute of Innovative Research, Tokyo Institute of Technology.

Conflicts of Interest: The authors declare no conflict of interest.

References

1. Strohmaier, K.G.; Reyes, S.C.; Levin, D. Preparation of High-Silica Chabazite Zeolites and Their Use in the Conversion of Oxygenates into Olefins. U.S. Patent 7,435,863, 12 December 2003.
2. Bhawe, Y.; Moliner-Marín, M.; Lunn, J.D.; Liu, Y.; Malek, A.; Davis, M. Effect of Cage Size on the Selective Conversion of Methanol to Light Olefins. *ACS Catal.* **2012**, *2*, 2490–2495. [[CrossRef](#)]
3. Andersen, P.J.; Bailie, J.E.; Casci, J.L.; Chen, H.Y.; Fedeyko, J.M.; Foo, R.K.S.; Rajaram, R.R. Transition Metal/Zeolite SCR [Selective Catalytic Reduction] Catalysts. U.S. Patent 20,100,290,963 A1, 18 November 2010.

4. Bull, I.; Boorse, R.S.; Jaglowski, W.M.; Koerner, G.S.; Moini, A.; Patchett, J.A.; Xue, W.; Burk, P.; Dettling, J.C.; Caudle, M.T. Copper CHA Zeolite Catalysts. WO 2,008,106,519 A1, 27 February 2008.
5. Zhao, R.; Zhao, Z.; Li, S.; Zhang, W. Insights into the Correlation of Aluminum Distribution and Bronsted Acidity in H-Beta Zeolites from Solid-State NMR Spectroscopy and DFT Calculations. *J. Phys. Chem. Lett.* **2017**, *8*, 2323–2327. [[CrossRef](#)] [[PubMed](#)]
6. Bourgogne, M.; Guth, J.L.; Wey, R. Process for the Preparation of Synthetic Zeolite, and Zeolites Obtained by Saeed Process. U.S. Patent 4,503,024, 5 March 1985.
7. Zones, S.I. Zeolite SSZ-13 and Its Method of Preparation. U.S. Patent 4,544,538, 1 October 1985.
8. Eilertsen, E.A.; Arstad, B.; Svelle, S.; Lillerud, K.P. Single parameter synthesis of high silica CHA zeolites from fluoride media. *Microporous Mesoporous Mater.* **2012**, *153*, 94–99. [[CrossRef](#)]
9. Vattipalli, V.; Paracha, A.M.; Hu, W.; Chen, H.; Fan, W. Broadening the Scope for Fluoride-Free Synthesis of Siliceous Zeolites. *Angew. Chem. Int. Ed.* **2018**, *57*, 3607–3611. [[CrossRef](#)] [[PubMed](#)]
10. Santilli, D.S.; Zones, S.I. Selective Conversion of Methanol to Low Molecular Weight Olefins over High Silica SSZ-13 Zeolite. U.S. Patent 4,496,786, 29 January 1985.
11. Eilertsen, E.A.; Nilsen, M.H.; Wendelbo, R.; Olsbye, U.; Lillerud, K.P. Synthesis of high silica CHA zeolites with controlled Si/Al ratio. *Stud. Surf. Sci. Catal.* **2008**, *174*, 265–268.
12. Deimund, M.A.; Harrison, L.; Lunn, J.D.; Liu, Y.; Malek, A.; Shayib, R.; Davis, M.E. Effect of Heteroatom Concentration in SSZ-13 on the Methanol-to Olefins Reaction. *ACS Catal.* **2016**, *6*, 542–550. [[CrossRef](#)]
13. Zhu, Q.; Kondo, J.N.; Ohnuma, R.; Kubota, Y.; Yamaguchi, M.; Tatsumi, T. The study of methanol-to-olefin over proton type aluminosilicate CHA zeolite. *Microporous Mesoporous Mater.* **2008**, *112*, 153–161. [[CrossRef](#)]
14. Kubota, Y.; Inagaki, S.; Fukuoka, T. Production of High Si/Al Ratio CHA-Type Zeolite. JP2016169118A, 23 September 2016.
15. Bohstrom, Z.; Arstad, B.; Lillerud, K.P. Preparation of high silica chabazite with controllable particle size. *Microporous Mesoporous Mater.* **2014**, *195*, 294–302. [[CrossRef](#)]
16. Zones, S.I. Conversion of Faujasites to High-silica Chabazite SSZ-13 in the Presence of N,N,N-Trimethyl-1-adamantammonium Iodide. *J. Chem. Soc. Faraday Trans.* **1991**, *87*, 3709–3716. [[CrossRef](#)]
17. Zones, S.I.; Van Nordstrand, R.A. Novel zeolite transformations: The template-mediated conversion of Cubic P zeolite to SSZ-13. *ZEOLITES* **1988**, *8*, 166–174. [[CrossRef](#)]
18. Zones, S.I. Preparation of molecular sieves using a structure directing agent and an N,N,N-triaryl benzyl quaternary ammonium cation. U.S. Patent 20,080,075,656, 25 September 2008.
19. Itakura, M.; Inoue, T.; Takahashi, A.; Fujitani, T.; Oumi, Y.; Sano, T. Synthesis of High-silica CHA Zeolite from FAU Zeolite in the Presence of Benzyltrimethylammonium Hydroxide. *Chem. Lett.* **2008**, *37*, 908–909. [[CrossRef](#)]
20. Itaura, M.; Goto, I.; Takahashi, A.; Fujitani, T.; Ida, Y.; Sadakane, M.; Sano, T. Synthesis of high silica CHA-type zeolite by inter zeolite conversion of FAU-type zeolite in the presence of seed crystals. *Microporous Mesoporous Mater.* **2011**, *144*, 91–96. [[CrossRef](#)]
21. Yamanaka, N.; Itakura, M.; Kiyozumi, Y.; Ide, Y.; Sadakane, M.; Sano, T. Acid stability evaluation of CHA-type zeolites synthesized by interzeolite conversion of FAU-type zeolite and their membrane application for dehydration of acetic acid aqueous solution. *Microporous Mesoporous Mater.* **2012**, *158*, 141–147. [[CrossRef](#)]
22. Martin, N.; Moliner, M.; Corma, A. High yield synthesis of high-silica chabazite by combining the role of zeolite precursors and tetraethylammonium: SCR of NO_x. *Chem. Commun.* **2015**, *51*, 9965–9968. [[CrossRef](#)] [[PubMed](#)]
23. Bhadraa, B.N.; Seoa, P.W.; Khana, N.A.; Junb, J.W.; Kimb, T.W.; Kimb, C.U.; Jhunga, S.H. Conversion of Y into SSZ-13 zeolite in the presence of tetraethylammonium hydroxide and ethylene-to-propylene reactions over SSZ-13 zeolites. *Catal. Today* **2017**, *298*, 53–60. [[CrossRef](#)]
24. Takata, T.; Tsumoji, N.; Takamitsu, Y.; Sadakane, M.; Sano, T. Incorporation of various heterometal atoms in CHA zeolites by hydrothermal conversion of FAU zeolite and their performance for selective catalytic reduction of NO_x with ammonia. *Microporous Mesoporous Mater.* **2017**, *246*, 89–101. [[CrossRef](#)]
25. Takata, T.; Tsumoji, N.; Takamitsu, Y.; Sadakane, M.; Sano, T. Nanosized CHA zeolites with high thermal and hydrothermal stability derived from the hydrothermal conversion of FAU zeolite. *Microporous Mesoporous Mater.* **2016**, *225*, 524–533. [[CrossRef](#)]

26. Xiong, X.; Yuan, D.; Wu, Q.; Chen, F.; Meng, X.; Lv, R.; Dai, D.; Maurer, S.; McGuire, R.; Feyen, M.; et al. Efficient and rapid transformation of high silica CHA zeolite from FAU zeolite in the absence of water. *J. Mater. Chem. A* **2017**, *5*, 9076–9080. [[CrossRef](#)]
27. Suji, K.; Wagner, P.; Davis, M.E. High-silica molecular sieve syntheses using the sparteine related compounds as structure-directing agents. *Microporous Mesoporous Mater.* **1999**, *28*, 461–469. [[CrossRef](#)]
28. Li, Y.; Zhang, Y.; Lan, A.; Bian, H.; Liu, R.; Li, X.; Han, P.; Dou, T. Synthesis of SSZ-13 zeolite with zeolite L-added synthesis gel absent from additional aluminum source. *Microporous Mesoporous Mater.* **2019**, *279*, 1–9. [[CrossRef](#)]
29. Tang, L.; Haw, K.G.; Zhang, Y.; Fang, Q.; Qiu, S.; Valtchev, V. Fast and efficient synthesis of SSZ-13 by interzeolite conversion of Zeolite Beta and Zeolite L. *Microporous Mesoporous Mater.* **2019**, *280*, 306–314. [[CrossRef](#)]
30. Geng, H.; Li, G.; Liu, D.; Liu, C. Rapid and efficient synthesis of CHA-type zeolite by interzeolite conversion of LTA-type zeolite in the presence of N, N, N-trimethyladamantammonium hydroxide. *J. Solid State Chem.* **2018**, *265*, 193–199. [[CrossRef](#)]
31. Yoshikawa, M.; Wagner, P.; Lovallo, M.; Tsuji, K.; Takewaki, T.; Chen, C.-Y.; Beck, L.W.; Jones, C.; Tsapatsis, M.; Zons, S.I.; et al. Synthesis, Characterization, and Structure Solution of CIT-5, a New, High-Silica, Extra-Large-Pore Molecular Sieve. *J. Phys. Chem. B* **1998**, *102*, 7139–7142. [[CrossRef](#)]
32. Muraoka, K.; Chaikittisilp, W.; Tatsuya Okubo, T. Energy Analysis of Aluminosilicate Zeolites with Comprehensive Ranges of Framework Topologies, Chemical Compositions, and Aluminum Distributions. *J. Am. Chem. Soc.* **2016**, *138*, 6184–6193. [[CrossRef](#)]
33. Honda, K.; Yashiki, A.; Itakura, M.; Ide, Y.; Sadakane, M.; Sano, T. Influence of seeding on FAU-*BEA interzeolite conversions. *Microporous Mesoporous Mater.* **2011**, *142*, 161–167. [[CrossRef](#)]
34. Goel, S.; Zones, S.I.; Iglesia, E. Encapsulation of Metal Clusters within MFI via Interzeolite Transformations and Direct Hydrothermal Syntheses and Catalytic Consequences of Their Confinement. *J. Am. Chem. Soc.* **2014**, *136*, 15280–15290. [[CrossRef](#)]
35. Li, C.; Moliner, M.; Corma, A. Building Zeolites from Precrystallized Units: Nanoscale Architecture. *Angew. Chem. Inter. Ed.* **2018**, *57*, 15330–15353. [[CrossRef](#)]
36. Goel, S.; Zones, S.I.; Iglesia, E. Synthesis of Zeolites via Interzeolite Transformations without Organic Structure-Directing Agents. *Chem. Mater.* **2015**, *27*, 2056–2066. [[CrossRef](#)]
37. Inoue, T.; Itakura, M.; Jon, H.; Oumi, Y.; Takahashi, A.; Fujitani, T.; Sano, T. Synthesis of LEV zeolite by interzeolite conversion method and its catalytic performance in ethanol to olefins reaction. *Microporous Mesoporous Mater.* **2009**, *122*, 149–154. [[CrossRef](#)]
38. Joichi, Y.; Shimono, D.; Tsunaji, N.; Takamitsu, Y.; Sadakane, M.; Sano, T. Stepwise Gel Preparation for High-Quality CHA Zeolite Synthesis: A Common Tool for Synthesis Diversification. *Cryst. Growth Des.* **2018**, *18*, 5652–5662. [[CrossRef](#)]
39. Nakazawa, N.; Inagaki, S.; Kubota, Y. Novel Technique to Synthesize AFX-Type Zeolite Using a Bulky and Rigid Diquaternary Ammonium Cation. *Adv. Porous Mater.* **2016**, *4*, 219–229. [[CrossRef](#)]
40. Peng, C.; Liu, Z.; Horimoto, A.; Anand, C.; Yamada, H.; Ohara, K.; Sukenaga, S.; Ando, M.; Shibata, H.; Takewaki, T.; et al. Preparation of nanosized SSZ-13 zeolite with enhanced hydrothermal stability by a two-stage synthetic method. *Microporous Mesoporous Mater.* **2018**, *255*, 192–199. [[CrossRef](#)]
41. Dusselier, M.; Davis, M.E. Small-Pore Zeolites: Synthesis and Catalysis. *Chem. Rev.* **2018**, *118*, 5265–5329. [[CrossRef](#)]
42. Nishitoba, T.; Yoshida, N.; Kondo, J.N.; Yokoi, T. Control of Al Distribution in the CHA-Type Aluminosilicate Zeolites and Its Impact on the Hydrothermal Stability and Catalytic Properties. *Ind. Eng. Chem. Res.* **2018**, *57*, 3914–3922. [[CrossRef](#)]
43. Lippmaa, E.; Satnoson, M.M.A.; Engelhardt, G.; Grimmer, A.R. Structural Studies of Silicates by Solid-state High-Resolution ²⁹Si NMR. *J. Am. Chem. Soc.* **1980**, *102*, 4889–4893. [[CrossRef](#)]
44. Iwama, M.; Suzuki, Y.; Plévert, J.; Itabashi, K.; Ogura, M.; Okubo, T. Location of Alkali Ions and their Relevance to Crystallization of Low Silica X Zeolite. *Cryst. Growth Des.* **2010**, *10*, 3471–3479. [[CrossRef](#)]
45. Mousavi, S.F.; Jafari, M.; Kazemimoghadam, M.; Mohammadi, T. Template free crystallization of zeolite Rho via Hydrothermal synthesis: Effects of synthesis time, synthesis temperature, water content and alkalinity. *Ceram. Int.* **2013**, *39*, 7149–7158. [[CrossRef](#)]

46. Bronic, J.; Palcic, A.; Subotic, B.; Itani, L.; Valtchev, V. Influence of alkalinity of the starting system on size and morphology of the zeolite A crystals. *Mater. Chem. Phys.* **2012**, *132*, 973–976. [[CrossRef](#)]
47. Ong, L.H.; Domok, M.; Olindo, R.; van Veen, A.C.; Lercher, J.A. Dealumination of HZSM-5 via steam-treatment. *Microporous Mesoporous Mater.* **2012**, *164*, 9–20. [[CrossRef](#)]
48. Wang, C.M.; Wang, Y.D.; Xie, Z.K. Insights into the reaction mechanism of methanol-to-olefins conversion in HSAPO-34 from first principles: Are olefins themselves the dominating hydrocarbon pool species? *J. Catal.* **2013**, *301*, 8–19. [[CrossRef](#)]
49. Li, C.; Paris, C.; Triguero, J.M.; Boronat, M.; Moliner, M.; Corma, A. Synthesis of reaction-adapted zeolites as methanol-to-olefins catalysts with mimics of reaction intermediates as organic structure directing agents. *Nat. Catal.* **2018**, *1*, 547–554. [[CrossRef](#)]
50. Kim, W.; So, J.; Choi, S.-W.; Liu, Y.; Dixit, R.S.; Sievers, C.; Sholl, D.S.; Nair, S.; Jones, C.W. Hierarchical Ga-MFI Catalysts for Propane Dehydrogenation. *Chem. Mater.* **2017**, *29*, 7213–7222. [[CrossRef](#)]
51. Xie, Y.; Hua, W.; Yue, Y.; Gao, Z. Dehydrogenation of propane to propylene over Ga₂O₃ supported on mesoporous HZSM-5 in the presence of CO₂. *J. Chem.* **2010**, *28*, 1559–1564.
52. Svelle, S.; Joensen, F.; Nerlov, J.; Olsbye, U.; Lillerud, K.P.; Kolboe, S.; Bjorgen, M. Conversion of Methanol into Hydrocarbons over Zeolite H-ZSM-5: Ethene Formation Is Mechanistically Separated from the Formation of Higher Alkenes. *J. Am. Chem. Soc.* **2006**, *128*, 14770–14771. [[CrossRef](#)]
53. Song, W.; Fu, H.; Haw, J.F. Supramolecular Origins of Product Selectivity for Methanol-to-Olefin Catalysis on HSAPO-34. *J. Am. Chem. Soc.* **2001**, *123*, 4749–4754. [[CrossRef](#)]

Publisher’s Note: MDPI stays neutral with regard to jurisdictional claims in published maps and institutional affiliations.



© 2020 by the authors. Licensee MDPI, Basel, Switzerland. This article is an open access article distributed under the terms and conditions of the Creative Commons Attribution (CC BY) license (<http://creativecommons.org/licenses/by/4.0/>).